PHOTONICS Research

High-sensitivity, high-spatial-resolution distributed strain sensing based on a poly(methyl methacrylate) chirped fiber Bragg grating

Chengang Lyu,[1] Ziqi Liu,[1] Ziqiang Huo,[1] Chunfeng Ge,[2] Xin Cheng,[3,*] and Haw-Yaw Tam[3]

[1]School of Electrical and Information Engineering, Tianjin University, Tianjin 300072, China
[2]School of Precision Instruments and Opto-electronics Engineering, Tianjin University, Tianjin 300072, China
[3]Photonics Research Center, The Hong Kong Polytechnic University, Kowloon, Hong Kong, China
*Corresponding author: eechengx@polyu.edu.hk

Received 24 February 2020; revised 1 May 2020; accepted 12 May 2020; posted 13 May 2020 (Doc. ID 391160); published 5 June 2020

In this study, a high-sensitivity, high-spatial-resolution distributed strain-sensing approach based on a poly(methyl methacrylate) chirped fiber Bragg grating (CFBG) is proposed and experimentally demonstrated. Linearly chirped FBGs in a polymer optical fiber provide an alternative to the silica fiber owing to the lower Young's modulus, which can yield a higher stress sensitivity under the same external force. According to the spatial wavelength-encoded characteristic of the CFBG, a fully distributed strain measurement can be achieved by optical frequency-domain reflectometry. Through time-/space-resolved short-time Fourier transform, the applied force can be located by the beat frequency originated from the space-induced time delay and measured by the differential frequency offset originated from the strain-induced dispersion time delay. In a proof-of-concept experiment, a high spatial resolution of 1 mm over a gauge length of 40 mm and a strain resolution of 0.491 Hz/με were achieved.

https://doi.org/10.1364/PRJ.391160

1. INTRODUCTION

Optical-fiber-grating-based sensors are emerging as promising devices owing to their high stabilities, high reliabilities, and advanced multiplexing capabilities [1]. In recent years, the application of chirped fiber Bragg grating (CFBG) with a nonuniform modulation of the refractive index within the core of an optical fiber has attracted considerable attention [2].

For high-spatial-resolution strain-sensing applications, such as tactile perception and aircraft structural detection [3,4], CFBG behaving as a cascade of FBGs of different Bragg wavelengths is a promising candidate for fully distributed sensors owing to its large grating length, spatial dispersion characteristic, and large reflection bandwidth. The strain information is encoded into the wavelength-dependent reflection spectral range. To interrogate the reflection spectrum, an optical spectrum analyzer [5], Fabry–Perot filter [6], microwave photonic filter [7], and time-stretch frequency-domain reflectometry [8] have been used. However, the performances of these interrogation techniques are limited by either the lack of spatial resolution or high-speed data acquisition requirement. With the reasonable measurement time and considerably higher spatial resolution, optical frequency-domain reflectometry (OFDR) is a powerful method for the measurement of a small reflection signal in small-scale optical components [9]. The distributed strain information along the grating section of the CFBG can be reconstructed theoretically from the recorded temporal interference waveform and interrogated by means of OFDR in a Michelson interferometer. Therefore, it is possible to detect spatially resolved variations in strain with a resolution on the order of millimeters over the grating length.

In addition to the high spatial resolution, high sensitivity is another important factor for the distributed strain-sensing technology. In most cases, strain is due to the applied external force, so the strain sensing is actually a measurement of external force. According to Hooke's law, polymer materials have higher sensitivity to converting external force into internal strain of the optical fiber, compared with silica material. Therefore, the mechanical properties provide increased sensitivities to intrinsic polymer fiber sensors when they are used for lateral force, stress, and torque sensing. Recently, polymer materials such as CYTOP, TOPAS, and PMMA have been researched for polymer optical fiber (POF) fabrication and application. Liu *et al.* [10] reported an axial tensile experiment using PMMA FBGs with a maximum strain of 3.61%. Leal *et al.* [11] measured the torque of an elastic actuator's spring based on CYTOP FBG arrays in the strain range of thousands. Woyessa *et al.* reported a single-mode POF using ZEONEX/TOPAS for high-temperature sensing [12]. Leal *et al.* reported a diaphragm-embedded sensor applied on the pressure, force, and liquid level

assessment using CYTOP fibers [13]. Among these materials, PMMA was the preferred material for producing POF because of its relative ease of fabrication, high optical transparency in the visible region, and refractive index similar to that of a conventional silica optical fiber [14]. CFBGs in PMMA-based optical fibers are promising sensing devices owing to their fundamental mechanical advantages over silica fibers (73 GPa) including a lower Young's modulus (2.3 GPa) [15], higher elastic limit, simple installation in a narrow space, and improved biocompatibility for sensing applications [16]. Min *et al.* and Marques *et al.* have reported that the PMMA-based CFBG can be used as an average strain sensor with a good sensitivity [17,18].

In this study, distributed measurement of strains along the different stress points of a single PMMA CFBG is studied innovatively. We fabricate a single-mode PMMA POF using a unique core dopant, diphenyl disulfide (DPDS), providing both increase in core refractive index and photosensitivity. The fabrication method is reported in Ref. [19]. CFBGs are inscribed in the PMMA POF using a chirped phase mask. The ultraviolet (UV) light source is a 248 nm KrF excimer laser. Our aim is to study the distributed strain-sensing ability of this novel PMMA CFBG. Compared with silica CFBG in an experiment, PMMA CFBG shows that it could realize distributed strain sensing with a good agreement between the theory and the experiment. To the best of our knowledge, for the first time, we have achieved a high-spatial-resolution, high-sensitivity distributed strain-sensing based on a PMMA CFBG, with a spatial resolution of 1 mm over a gauge length of 40 mm and strain resolution of 0.491 Hz/με.

2. SCHEMATIC AND THEORY

Figure 1 illustrates the proposed approach. The PMMA CFBG wavelength spectrum of each grating section is different and unique in the free state. The proposed system as shown in Fig. 2 could be regarded as optical coherence tomography based on OFDR, which includes a swept laser source (SS), a Faraday rotator mirror (FRM) as a reference, and a PMMA CFBG as a sensing element.

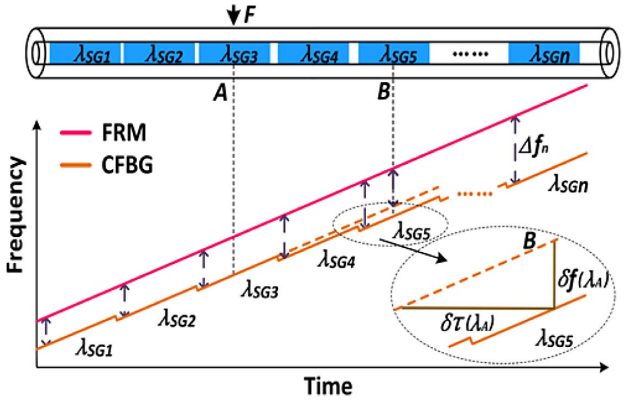

Fig. 1. Frequency relationship between the CFBG and FRM and corresponding beat frequencies. Inset: differential frequency offset $\delta f(\lambda_A)$ of the CFBG under strain. SG, grating section.

By beating the signals from the FRM and the PMMA CFBG at the photodetector (PD), beat signals $\Delta f_n(\lambda)$ with a microwave frequency dependent on the Bragg wavelength and proportional to the time-delay difference between the two reflected waveforms are generated, which could be used as a baseline to measure and locate the strain information along the PMMA CFBG:

$$\Delta f_n(\lambda) = f_{\mathrm{FRM}} - f_{\mathrm{CFBG}}(\lambda) = \alpha \times \Delta\tau(\lambda), \tag{1}$$

where α is the sweep rate, $\alpha = \Delta f / T$, where Δf is the sweep range and T is the sweep period; and $\Delta\tau(\lambda)$ is the distance-induced time delay $2nL/c$, owing to the different positions of the FRM and PMMA CFBG grating section.

Therefore, the beat signals generated by the time-delay difference correspond to the chirped dispersion wavelength and spatial position of the PMMA CFBG as shown in Fig. 1. For a given PMMA CFBG chirp rate and grating sensing length, the sweep range and period could be adjusted to provide a suitable measurement range output limited by the frequency response of the receiver.

A lateral force F applied at a certain position A on the PMMA CFBG produces an axial stress [20]

$$\sigma = 4\gamma F / \pi L D, \tag{2}$$

where γ is the Poisson's ratio of PMMA of 0.4, L is the lateral force zone, and D is the diameter of the optical fiber. The strain at this position can be expressed as

$$\Delta\varepsilon = \sigma / E, \tag{3}$$

where E is the Young's modulus of PMMA. The change in local strain $\Delta\varepsilon$ modifies the specific Bragg wavelength at the local position. Thus, the instantaneous Bragg wavelength shift at this position can be expressed as

$$\delta\lambda_A = \lambda_A(1 - P_e)\Delta\varepsilon, \tag{4}$$

where $\delta\lambda_A$ is the wavelength shift induced by the strain, P_e is the effective strain-optic coefficient of PMMA of 0.034, λ_A is the initial wavelength at a specific reflection position A in the PMMA CFBG, and $\Delta\varepsilon$ is the applied strain.

For the PMMA CFBG with a chirp rate of C_{chirp} [nanometers per centimeter (nm/cm)], by using Eq. (4), we obtain the relationship between the strain-induced dispersion time delay $\delta\tau(\lambda_A)$ and applied strain:

$$\delta\tau(\lambda_A) = \frac{2n}{cC_{\mathrm{chirp}}}\delta\lambda_A, \tag{5}$$

where n is the refractive index and c is the speed of light. The strain-induced differential frequency offset (DFO) is

$$\delta f(\lambda_A) = \alpha \times \delta\tau(\lambda_A). \tag{6}$$

As shown in Fig. 1, assuming that the Bragg wavelength at grating section A changes to the Bragg wavelength at grating section B under a specific lateral force, then the beat frequency at position A is time delayed to position B. So two beat signals would exist at the sampling time of position B. One is the original distance-induced beat signal at position B, and the other is strain-induced beat signal from position A. Therefore, the strain by lateral force at position A could be determined by measuring the DFO $\delta f(\lambda_A)$ between these two beat signals.

3. EXPERIMENTS AND ANALYSIS

An experiment is performed to verify the utility of the proposed technique. Figure 2 shows a schematic of the experimental setup in our laboratory based on a fiber-optical Michelson interferometer. The PMMA CFBG used in this experiment was manufactured at the Photonics Research Center, The Hong Kong Polytechnic University, Hong Kong SAR. The optical setup for chirped grating inscription is depicted in Fig. 3. Linear CFBGs are inscribed in DPDS-doped PMMA optical fibers using a UV KrF excimer laser operating at 248 nm. During the writing of the CFBGs, the repetition rate of the laser is 15 Hz, while the output energy of the laser is 50 mJ. A cylindrical lens shapes the beam before it arrives at the chirped phase mask (BRAGG Photonic Inc., 1067.17 ± 17.5 nm). The POF sections with a length of 30 cm are placed within two magnetic clamps and kept under strain to avoid undesired curvatures. The diameter of the laser beam is 2 mm, considerably smaller than the grating size (50 mm × 3 mm) on the phase mask. Thus, the beam scanning method is used in this process to achieve 40 mm long chirped Bragg gratings. The optimized scanning speed is 0.2 mm/s in this case. The PMMA CFBG has a chirp rate of 10 nm/cm and diameter of 120 μm.

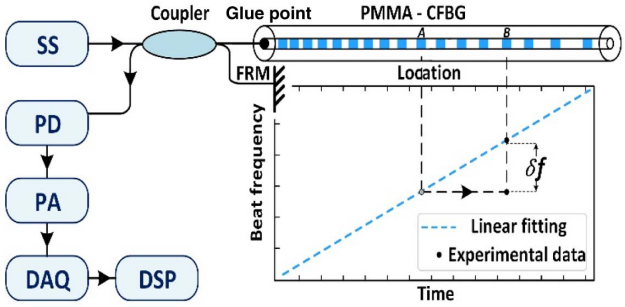

Fig. 2. Schematic of the experimental setup. Inset: beat frequency relationship between the time and position. The blue dotted line is the linear fit, which reflects the distance-induced beat frequency, while the black spots show the DFO. SS, swept laser source; PD, photodiode; PA, power amplifier; DAQ, data acquisition; DSP, digital signal processor.

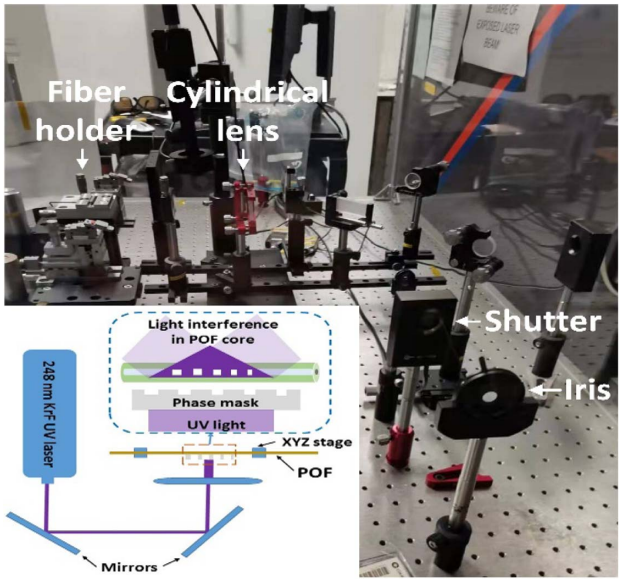

Fig. 3. Optical setup for chirped grating inscription.

To demonstrate the effectiveness and practicability of the proposed method, we experimentally compare the distributed strain-sensing abilities of silica CFBG and PMMA CFBG. According to the reflection bandwidths of both CFBGs, a swept laser source (Keysight 8164B) is adjusted and provides a linear wavelength modulation in the range of 1520–1620 nm with a sweep rate of 200 nm/s. The light wave from the swept laser source is sent to the FRM and CFBG through an isolator and a 3 dB fiber coupler with a weak wavelength-dependence loss. The short-wavelength end of the CFBG is connected to the coupler. The output of the interferometer with the wavelength-swept source produces beat signals at the PD (Thorlabs DET01CFC). The relative position of the FRM could be set before or after the CFBG according to the application, which only affects the increase or decrease in beat frequency in the same sweep direction, as shown by experiments. By adjusting the distance between the FRM and CFBG, the beat signals can be acquired by a low-speed data acquisition card (NI6010 200 kHz). A fully distributed strain along the CFBG could be measured through a time-/space-resolved short-term Fourier transform (STFT) analysis.

In the experiments, the resonance wavelength of the sensing silica-CFBG is centered at 1545 nm with a reflection bandwidth of 40 nm as shown in the upper inset of Fig. 4(a). The scanning measurement time covering the sensing silica CFBG is 200 ms at a sweep rate of 200 nm/s. The temporal interference waveform signals are detected by a PD and recorded using the data acquisition card by data sampling at 60 kHz. The lower inset of Fig. 4(a) shows the measured initial temporal interference waveform in the absence of applied strain. The spectrograms of the recorded waveforms are calculated using an STFT analysis. As shown in Fig. 4(a), the time-frequency distribution is in the range of 19.6–9.3 kHz, owing to the 40 mm length of the silica CFBG and 36 mm distance from the silica CFBG to the FRM, consistent with Eq. (1). In Fig. 4(b), the silica CFBG is replaced by the PMMA CFBG. The resonance wavelength of the sensing PMMA CFBG is centered at 1580 nm with a reflection bandwidth of 40 nm, owing to the increase in material refractive index, as shown in the upper inset of Fig. 4(b). The scanning measurement and signal sampling are unchanged. As shown in Fig. 4(b), the time-frequency distribution is in the range of 10.4–19.7 kHz, owing to the PMMA CFBG length of 40 mm and distance from the FRM to the PMMA CFBG of 40 mm. Compared to the silica-CFBG, although a higher noise is observed in the time-frequency distribution owing to the reflection magnitude response ripples of the PMMA CFBG, the linear fitting of the experimental signal of beat frequencies is in agreement with the principle of CFBG demodulation by OFDR, and it conforms to Eq. (1).

When an external lateral force is applied to the two types of CFBGs at a certain carrying position, their strain responses

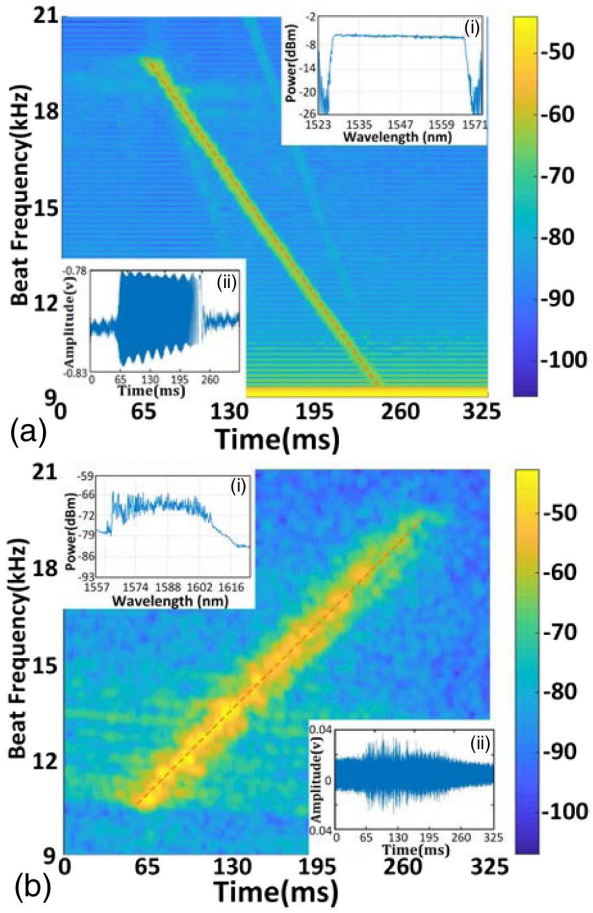

Fig. 4. Microwave spectrogram calculated by STFT without strain. (a) Silica fiber. (b) PMMA fiber. Insets: (i) measured reflection spectrum and (ii) measured initial temporal interference waveform.

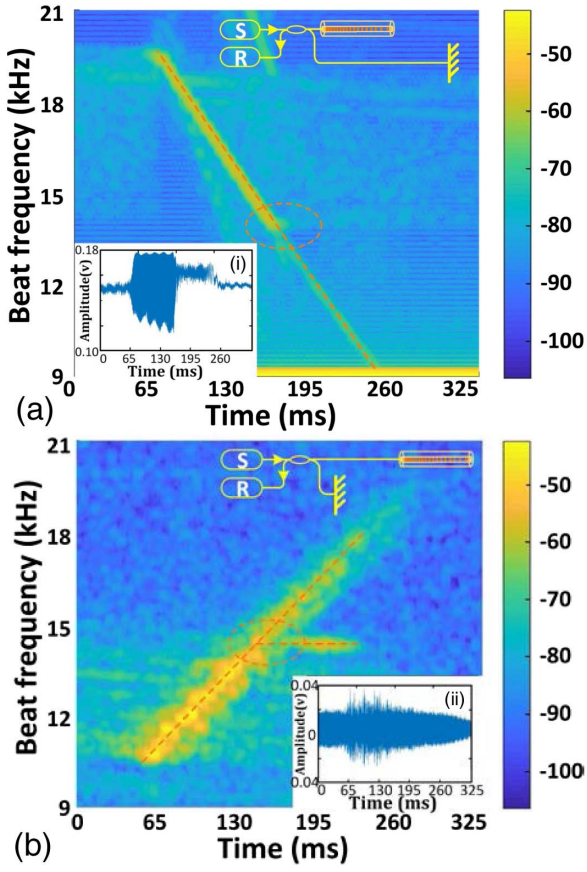

Fig. 5. Microwave spectrogram calculated by STFT under strain. (a) Silica fiber. (b) PMMA fiber. Insets: reflection spectra of the (i) silica and (ii) PMMA fibers under stress.

are different, owing to the different characteristics of the two materials. As shown in Fig. 5(a), we increase the lateral force over 50 N while preventing fiber breaking. Notably, no considerable DFO is observed in the spectrogram of the silica CFBG, even though the light entering the latter half of the CFBG is blocked by the large external force. For the PMMA CFBG, a considerable DFO is observed in the spectrogram under a lateral force smaller than 1 N, which could be used for quantitative calculation and positioning as shown in Fig. 5(b).

As shown in Fig. 6, when an external lateral force is applied to the PMMA CFBG at a carrying position of 16 mm from its short-wavelength end with a carrying zone of ~0.5 mm, the strain affects the grating section at this position according to Eqs. (2) and (3). Spectrograms of the two recorded waveforms are calculated by STFT and shown in the inset of Fig. 6 at uniform strains of 4060 and 5540 με. The strain-induced DFO is observed at a definite time of sweeping the whole waveform, which could be used to locate the strain position. Figure 6 shows the measured DFO as a function of the applied strain. When the strain is increased from 3000 to 7000 με, the DFO is shifted from approximately 1.50 to 3.50 kHz. The results in Fig. 6 confirm the expected linear relationship between the applied strain and the strain-induced DFO as predicted by Eqs. (4)–(6). The sensitivity estimated by linearly fitting the experimental data in Fig. 6 is 0.491 Hz/με. The result agrees well with the theoretical value of 0.5 Hz/με calculated using Eqs. (4)–(6), and the error rate between the experimental and theoretical data is 1.35%. As the strain measurement range of the POF is usually thousands of microstrain, this sensitivity could be consistent with the kilohertz sampling rates of most commercial data acquisition cards. In addition, the sensitivity can be improved by reducing the chirp rate of the PMMA CFBG and increasing the sweep speed according to the actual measurement range.

Considering the high strain sensitivity and high spatial resolution of the proposed technique, we analyze the capability of the PMMA CFBG to identify different stresses at different positions of the sensor grating. We glue the sensing PMMA CFBG on top of a substrate and simultaneously load stresses at different positions. As shown in Fig. 7, two points of the PMMA CFBG are loaded with external lateral stresses, which act as test points. Based on the above theory, two sudden instantaneous DFOs are expected at the specific times corresponding to the individual stress points.

Figures 7(a)–7(d) show the experimental results of spatial resolution between two stress points from 4 to 1 mm. According to Eq. (1), the theoretical spatial resolution is the

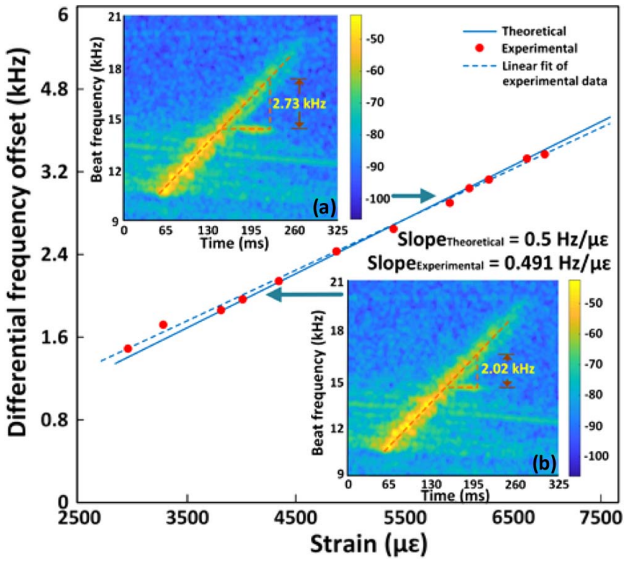

Fig. 6. DFO at various strains. The insets show spectrograms of the temporal interference patterns at uniform strains of 4060 and 5540 με.

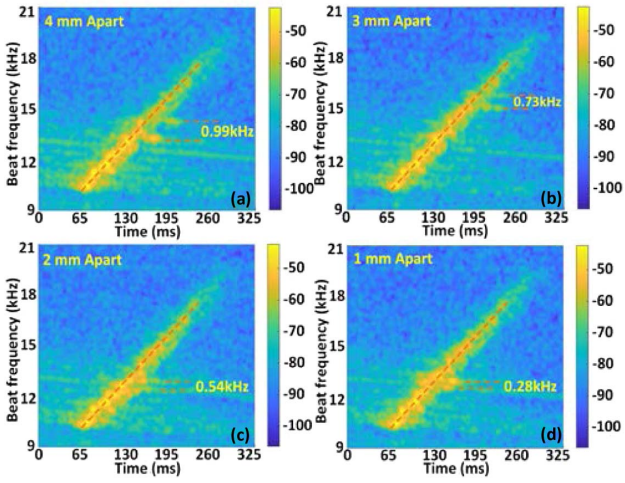

Fig. 7. Characterization of the system by applying various uniform strains at distances of (a) 4 mm, (b) 3 mm, (c) 2 mm, and (d) 1 mm.

frequency difference of two stress points of 0.25 kHz/mm. The original graphs of the experiments are shown here. Even with the SNR problems, the 1 mm resolution could still be seen in the experiment with 0.28 kHz, which is in good agreement with the theoretical value. Figure 8 shows the comparison of theoretical and experimental values of spatial resolution.

As we know, the quality of fiber drawn from preform can affect the quality of CFBG. So we think that the improvement on the preform must be investigated from the two aspects: the uniformity of the dopant in the core area must be improved, and the surface of the preform after processing must be smoother. According to the aforementioned information, in the future, we may try adding no extra dopant (in this paper, DPDS is the extra dopant) [12]. Therefore, by improving the

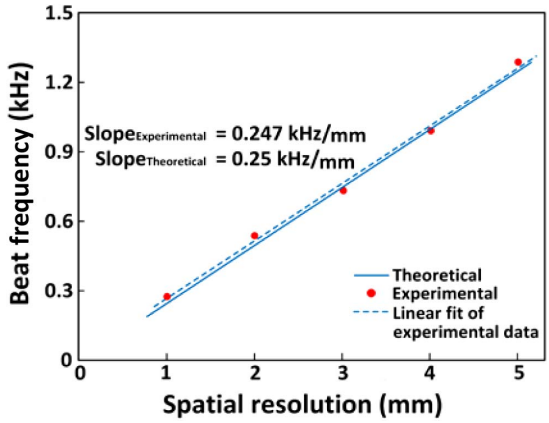

Fig. 8. Comparison of theoretical and experimental values of spatial resolution.

fabrication quality of PMMA CFBG devices, combined with the relevant filtering algorithm and other conditions to solve the SNR problems, it is believed that the spatial resolution ability is not limited to 1 mm with the method of this paper.

4. CONCLUSION

We propose and experimentally demonstrate a fully distributed strain-sensing approach using PMMA CFBG based on OFDR with high spatial resolution and sensitivity. The principle of the approach is to transform the distributed strain and location information along the grating length to the DFO through the distance-induced time delay and strain-induced dispersion time delay. The proposed technique is verified by experiments. A spatial resolution of 1 mm over a gauge length of 40 mm and a strain resolution of 0.491 Hz/με are achieved. One measurement cycle is about 200 ms according to the sweep rate of the light source in this paper. The spatial resolution depends on the reflection response ripples of the PMMA CFBG, while the strain resolution and demodulation speed depend on the chirp rate of the PMMA CFBG and sweep speed of the light source [21]. Considering the high sensitivity of the PMMA fiber, by improving the inscription quality of the CFBG and sweep rate of the light source and using a new material with a considerably lower Young's modulus for the POF, the proposed technique could be a promising distributed strain-sensing approach for short-range fully distributed sensing systems where high spatial resolution, sensitivity, and measurement speed are required.

Funding. The Hong Kong Polytechnic University (1-ZVGB); National Natural Science Foundation of China (61205075).

Disclosures. The authors declare that there are no conflicts of interest related to this paper.

REFERENCES

1. I. Floris, J. Madrigal, S. Sales, J. M. Adam, and P. A. Calderón, "Experimental study of the influence of FBG length on optical shape sensor performance," Opt. Laser. Eng. **126**, 105878 (2020).

2. X. Yang, R. Lindberg, W. Margulis, K. Fröjdh, and F. Laurell, "Continuously tunable, narrow-linewidth laser based on a semiconductor optical amplifier and a linearly chirped fiber Bragg grating," Opt. Express **27**, 14213–14220 (2019).
3. T. Li, C. Shi, and H. Ren, "A high-sensitivity tactile sensor array based on fiber Bragg grating sensing for tissue palpation in minimally invasive surgery," IEEE/ASME Trans. Mechatronics **23**, 2306–2315 (2018).
4. A. Ghoshal, J. Ayers, M. Gurvich, M. Urban, and N. Bordick, "Experimental investigations in embedded sensing of composite components in aerospace vehicles," Composites Part B **71**, 52–62 (2015).
5. J. He, S. Yang, and Q. Wei, "Intensity-modulated magnetic field sensor based on fiber Bragg grating," AIP Adv. **9**, 105303 (2019).
6. H. Xia, C. Zhang, H. Mu, and D. Sun, "Edge technique for direct detection of strain and temperature based on optical time domain reflectometry," Appl. Opt. **48**, 189–197 (2009).
7. O. Xu, J. Zhang, and J. Yao, "High speed and high resolution interrogation of a fiber Bragg grating sensor based on microwave photonic filtering and chirped microwave pulse compression," Opt. Lett. **41**, 4859–4862 (2016).
8. E. J. Ahmad, C. Wang, D. Feng, Z. Yan, and L. Zhang, "High temporal and spatial resolution distributed fiber Bragg grating sensors using time-stretch frequency-domain reflectometry," J. Lightwave. Technol. **35**, 3289–3295 (2016).
9. K. Yuksel, V. Moeyaert, P. Mégret, and M. Wuilpart, "Complete analysis of multireflection and spectral-shadowing crosstalks in a quasi-distributed fiber sensor interrogated by OFDR," IEEE Sens. J. **12**, 988–995 (2011).
10. H. Liu, H. Liu, and G. Peng, "Tensile strain characterization of polymer optical fibre Bragg gratings," Opt. Commun. **251**, 37–43 (2005).
11. A. G. Leal-Junior, A. Theodosiou, R. Min, J. Casas, C. R. Díaz, W. M. Dos Santos, M. J. Pontes, A. A. Siqueira, C. Marques, and K. Kalli, "Quasi-distributed torque and displacement sensing on a series elastic actuator's spring using FBG arrays inscribed in CYTOP fibers," IEEE Sens. J. **19**, 4054–4061 (2019).
12. G. Woyessa, A. Fasano, A. Stefani, C. Markos, and O. Bang, "Single mode step-index polymer optical fiber for humidity insensitive high temperature fiber Bragg grating sensors," Opt. Express **24**, 1253–1260 (2016).
13. A. G. Leal-Junior, H. R. O. Rocha, A. Theodosiou, A. Frizera, C. Marques, K. Kalli, and M. R. N. Ribeiro, "Optimizing linearity and sensitivity of 3D-printed diaphragms with chirped FBGs in CYTOP fibers," IEEE Access **8**, 31983–31991 (2018).
14. A. R. Prado, A. G. Leal-Junior, C. Marques, S. Leite, G. L. De Sena, L. C. Machado, A. Frizera, M. R. Ribeiro, and M. J. Pontes, "Polymethyl methacrylate (PMMA) recycling for the production of optical fiber sensor systems," Opt. Express **25**, 30051–30060 (2017).
15. X. Cheng, Y. Liu, and C. Yu, "Gas pressure sensor based on BDK-doped polymer optical fiber," Micromachines **10**, 717 (2019).
16. J. Bonefacino, X. Cheng, C.-F. J. Pun, S. T. Boles, and H.-Y. Tam, "Impact of high UV fluences on the mechanical and sensing properties of polymer optical fibers for high strain measurements," Opt. Express **28**, 1158–1167 (2020).
17. R. Min, B. Ortega, and C. Marques, "Fabrication of tunable chirped mPOF Bragg gratings using a uniform phase mask," Opt. Express **26**, 4411–4420 (2018).
18. C. Marques, P. Antunes, P. Mergo, D. Webb, and P. André, "Chirped Bragg gratings in PMMA step-index polymer optical fiber," IEEE Photon. Technol. Lett. **29**, 500–503 (2017).
19. J. Bonefacino, H.-Y. Tam, T. S. Glen, X. Cheng, C.-F. J. Pun, J. Wang, P.-H. Lee, M.-L. V. Tse, and S. T. Boles, "Ultra-fast polymer optical fibre Bragg grating inscription for medical devices," Light Sci. Appl. **7**, 17161 (2018).
20. R. Gafsi and M. A. El-Sherif, "Analysis of induced-birefringence effects on fiber Bragg gratings," Opt. Fiber. Technol. **6**, 299–323 (2000).
21. A. P. Hilton, P. S. Light, L. Talbot, and A. N. Luiten, "Optimal design for spectral narrowing and fast frequency sweep of an interferometer-stabilized laser," Opt. Lett. **45**, 45–48 (2020).